Collisional Effects in Non-stationary Plasma Expansions along Convergent-Divergent Magnetic Nozzles

J. Zhou[1,3], G. Sánchez-Arriaga[1], E. Ahedo[1], M. Martínez-Sánchez[2] and J. Ramos[1]
[1]Equipo de Propulsión Espacial y Plasmas, Universidad Carlos III de Madrid, 28911 Leganés, Spain, Email[3]: jiewei.zhou@uc3m.es
[2]Department of Aeronautics and Astronautics, Massachusetts Institute of Technology, Cambridge, 02139, Massachusetts, USA

KEYWORDS:

Magnetic nozzles, Boltzmann equation, weakly collisional plasmas

ABSTRACT:

The electron-electron collisional effect on the non-stationary expansion of a plasma in a convergent-divergent magnetic nozzle is studied. Under paraxial and fully magnetized plasmas approximations, an Eulerian code has been adapted to solve Poisson's equation coupled with the kinetic transport equations for plasma species, i.e. a Vlasov equation for singly-charged ions and a Boltzmann equation with a Bhatnagar-Gross-Kook operator for electrons. The study is focused on weakly collisional plasma plumes, which have a collisional time scale larger than the transit time in the nozzle of typical electrons. A kinetic analysis shows that phase-space regions of isolated, doubly-trapped electrons that are nearly empty in the collisionless case are progressively populated due to the electron-electron collisions. Such a higher density of trapped electrons modifies the profile of the electrostatic potential, which keeps almost unaltered the density of free electrons and decreases the density of the reflected ones. As compared with the collisionless case, the collisions decrease the length of the downstream sheath and the parallel electron temperature while increasing the normal one. Therefore the steady plasma state is more isotropic. The simulations show that collisions erase the time history of the system and, unlike the collisionless case, the steady state is unique.

1. INTRODUCTION

Many astrophysical scenarios, and also some engineering devices such as magnetic nozzles, involve the expansion of a plasma from a source into the vacuum and in the presence of a magnetic field. In many of them, the collision frequency is so low as compared with other characteristic times of the system, that the plasma expansion can be taken as collisionless. However, in the very long term, the effect in the steady state of such rare collisions is unclear. This is particularly interesting for the phase-space regions occupied by particles that are doubly-trapped between two axial coordinates. In a collisionless plasma, these special regions are populated during the transient phase and plasma species injected from the source cannot access them in the steady state. Collisions, even if they are rare, can slowly populate them and change the final steady state. Fluid models cannot describe correctly this trapping phenomenon in weakly collisional plasmas and a kinetic description is necessary. Self-consistent solutions of the stationary Vlasov-Poisson system has been obtained for a magnetic nozzle with slender geometry [1]. Since a stationary model cannot provide rigorously the amount of particles trapped during the transient, the authors added an heuristic population and found that the steady state solution was sensitive to the particular choice. In a recent work, the non-stationary expansion of a collisionsless plasma in a paraxial magnetic nozzle was studied numerically [2]. Vlasov simulations showed that both the electron trapping and the steady state of the plasma depend on the transient phase. Therefore, it was concluded that the final state of a collisionless plasma expansion depends on the history of the system.
In this work, we add collisional effects and study the plasma expansion though numerical simulations of the Boltzmann equation. The purpose of the study is twofold. In the first place, it reveals the impact of the collisions on macroscopic quantities, such as electric potential, plasma densities and temperatures, and also some kinetic features such as trapped particle population. In addition, non-stationary Boltzmann simulations can give insight into an interesting theoretical question: do collisional effects make collapse to the same state all the steady states of collisionless plasma expansions in magnetic nozzles ? The answer to this question clarifies whether or not, in the long term, collisions erase completely the history of the plasma expansion and make the steady state independent on the transient phase.

2. MAGNETIC NOZZLE MODEL

Besides collisions, the physical configuration of the plasma expansion and the numerical method used in this work are similar to the ones introduced in

Ref. [2]. For this reason, this section presents briefly the most important features of the model and pays special attention to the differences introduced by the collisions. Interested readers can find more details in Appendix A and Ref. [2].

2.1. Plasma Model

An infinitely large tank placed at $z < z_0 < 0$ is filled with an electron-ion plasma. At $z > z_0$ there is vacuum and an external magnetic field generated by a current loop of radius R_L placed at $z = 0$. Such a magnetic field is stationary and non-uniform and it reaches its maximum value B_T at $z = 0$ (the nozzle throat T). Suddenly, the nozzle is started and the plasma of the tank expands into the vacuum. There are several possibilities for the forward distribution functions of ions and electrons entering the nozzle. For simplicity, we will assume here that they are semi-Maxwellian,

$$f_\alpha(t, z=z_0, v_\parallel > 0, v_\perp) = \chi_\alpha(t) N^* \left(\frac{m_\alpha}{2\pi T_\alpha^*}\right)^{3/2} \exp\left(-\frac{m_\alpha v^2}{2T_\alpha^*}\right), \qquad \alpha = i, e \qquad \text{(Eq. 1)}$$

with subscript $\alpha = e$ and $\alpha = i$ referring to electrons and ions. Therefore, we assume a fully ionized plasma without neutrals. Parameters with a star denote reference parameters such as particle density N^* and temperature T_α^*. However, these are not the actual densities and temperatures at $z = z_0$, because they also involve the backward distribution functions that are computed self-consistently by the code. For convenience, we write the velocity as $v = \sqrt{v_\parallel^2 + v_\perp^2}$ with $v_\parallel$ and $v_\perp$ the velocity component parallel and normal to the magnetic field lines. Finally the paramenter $\chi_\alpha(t)$ is $\chi_e = 1$ for electrons and $\chi_i(t)$ is adjusted dynamically for ions to accomplish quasineutrality at the entrance $z = z_0$. We will follow the nomenclature of Ref. [2] and axial coordinate, time, velocities, magnetic field, electrostatic potential, particle distribution functions, and densities, are normalized according to $z/\lambda_{De}^* \to z$, $t\omega_{pe}^* \to t$, $v_{\parallel,\perp}/\lambda_{De}^*\omega_{pe}^* \to v_{\parallel,\perp}$, $B/B_T \to B$, $e\phi/k_B T_e^* \to \phi$, $f_\alpha/N^*\left(m_e/k_B T_e^*\right)^{3/2} \to f_\alpha$, where $\lambda_{De}^* = \sqrt{\epsilon_0 k_B T_e^*/N^* e^2}$ is the Debye length, $\omega_{pe}^* = \sqrt{N^* e^2/m_e\epsilon_0}$ the electron plasma frequency, k_B the Boltzmann constant, m_e the electron mass, e the elementary charge, and ϵ_0 the vacuum permitivity.

The models assumes a slender and slowly-varying magnetic field and the analysis is focus at the center line of the nozzle. The normalized magnetic field as a function of the axial distance at the axis of the nozzle then reads

$$\boldsymbol{B}(z) = \frac{r_L^3}{\left(r_L^2 + z^2\right)^{3/2}} \mathbf{1}_z, \qquad \text{(Eq. 2)}$$

where $\mathbf{1}_z$ is an unit vector along the z-axis and $r_L \equiv R_L/\lambda_{De}^*$. We will also assume that the magnetic field is very strong, i.e. the Larmor radius satisfies $\rho_{L\alpha} \equiv \beta v_\perp/|Z_\alpha|B << r_L$, and the plasma particles are fully attached to the magnetic field lines. Therefore, the normalized magnetic moment $\mu_\alpha = \beta_\alpha v_\perp^2/2B$ is conserved. Here $\beta_\alpha \equiv m_\alpha/m_e$ and Z_α are the mass and the charge number of the α-species. The effect of the induced magnetic field will be also ignored. Under this set of hypotheses, the gyrocenter distribution functions $\bar{f}_\alpha$, i.e.the distribution functions averaged over the fast gyrophase, are governed by the Boltzmann equations

$$\frac{\partial \bar{f}_\alpha}{\partial t} + v_\parallel \frac{\partial \bar{f}_\alpha}{\partial z} + a_\alpha \frac{\partial \bar{f}_\alpha}{\partial v_\parallel} = Q_\alpha\left(\bar{f}_e, \bar{f}_i\right), \qquad \text{(Eq. 3)}$$

where Q_α is a collisional operator, and we introduced the normalized acceleration

$$a_\alpha = -\frac{1}{\beta_\alpha}\left(Z_\alpha \frac{\partial \phi\left(t,z\right)}{\partial z} + \mu \frac{dB\left(z\right)}{dz}\right) \qquad \text{(Eq. 4)}$$

with Z_α the charge number. Such acceleration involves the electric field $\boldsymbol{E} = E_\parallel \boldsymbol{B}/B = -\partial\phi/\partial z$, which is given by the paraxial Poisson's equation

$$B\frac{\partial}{\partial z}\left(\frac{E_\parallel}{B}\right) = \sum_{\alpha=e,i} Z_\alpha n_\alpha \qquad \text{(Eq. 5)}$$

and the densities computed from the distribution functions as

$$n_\alpha(z) = \int f_\alpha d\boldsymbol{v} = \frac{2\pi B}{\beta_\alpha}\int_{-\infty}^{+\infty}\int_0^{+\infty} \bar{f}_\alpha dv_\parallel d\mu. \qquad \text{(Eq. 6)}$$

Particle collisions are modeled by the Bhatnagar-Gross-Kook operator [3]

$$Q_\alpha^{BGK} = \frac{1}{\tau_\alpha}\left[\bar{f}_{M\alpha}\left(n_\alpha, u_\alpha, T_\alpha\right) - \bar{f}_\alpha\right] \qquad \text{(Eq. 7)}$$

with τ_α a normalized collision time. Such a operator, which is not rigorous but useful to gain insight into the physics of the expansion, pushes the actual distribution function $\bar{f}_\alpha$ towards the function

$$\bar{f}_{M\alpha}\left(n_\alpha, u_\alpha, T_\alpha\right) = n_\alpha\left(\frac{\beta_\alpha}{2\pi T_\alpha}\right)^{3/2} \exp\left[-\frac{\beta_\alpha\left(v_\parallel - u_\alpha\right)^2}{2T_\alpha} - \frac{B\mu}{T_\alpha}\right], \qquad \text{(Eq. 8)}$$

which is a Maxwellian distribution function with the same density n_α, mean velocity along the magnetic field line u_α, and temperature T_α, as the actual distributions $\bar{f}_\alpha$. The density is given by Eq. 6, and the mean velocity $u_\alpha = \left\langle v_\parallel \right\rangle_\alpha$ and temperature $T_\alpha = (T_{\parallel\alpha} + 2T_{\perp\alpha})/3$ are found straightforwardly after introducing the average or mean value of any

quantity ψ as

$$\langle\psi\rangle_\alpha = \frac{1}{n_\alpha}\int \psi \bar{f}_\alpha d\boldsymbol{v} = \frac{2\pi B}{\beta_\alpha n_\alpha}\int_{-\infty}^{+\infty}\int_0^{+\infty}\psi\bar{f}_\alpha dv_\parallel d\mu, \qquad \text{(Eq. 9)}$$

with $T_{\parallel\alpha} = \beta_\alpha \left\langle c_{\parallel\alpha}^2 \right\rangle_\alpha$, $c_{\parallel\alpha} = v_\parallel - u_\alpha$ the peculiar velocity, and $T_{\perp\alpha} = B\langle\mu\rangle_\alpha$.

2.2. Setup of the Simulations

The VLAsov Simulator for MAgnetic Nozzles (VLASMAN), explained in detail in Ref. [2], has been extended to include collisions and solve (Eq. 3) and (Eq. 5). Unlike particle-in-cell simulators, which use macroparticles, VLASMAN is an Eulerian code that solves the kinetic equation on a finite grid of phase space, i.e. $z_0 \le z \le z_M$, $-v_{max}^\alpha \le v_\parallel \le v_{max}^\alpha$ and $0 \le \mu \le \mu_{max}^\alpha$. Consequently, it is computationally demanding but provides a high precision in regions where the distribution function is small, as it naturally happens in a plasma expansion to the vacuum. The main differences of the extended version of the code include the implementation of the collision operator (see details in Appendix A) and the μ-grid. Since the magnetic moment grid is constructed in a finite domain $0 \le \mu \le \mu_{max}^\alpha$, the truncation value μ_{max} should be high enough to ensure that the distribution function is small at the boundaries. Otherwise, the boundary condition $f(t, z, v_\parallel, \mu > \mu_{max}) = 0$ imposed by the code would yield wrong results. Our collision operator in (Eq. 7) involves the Maxwellian distribution function with the exponential of $-B\mu/T_e$ [see (Eq. 8)]. For large z, the magnetic field is very small [see (Eq. 2)] and a high value of μ is needed to capture correctly the Maxwellian. For this reason, we set the computational box limits to $z_0 = -10$ and $z_M = 100$ (smaller than the one used in Ref. [2]), increased the value of μ_{max}^e up to 105, and implemented a nonuniform grid distribution in μ. For electrons, a total of 40 grid points were distributed uniformly from $0 \le \mu \le 5.6$ and 41 non-equispaced points were used in the interval $5.6 < \mu \le \mu_{max}^e$. Ions are not problematic because we ignored their collisions. Such strategy provides enough resolution in the region of interest, where most of the trapping process occurs, and also captures correctly the behavior of the Maxwellian distribution function appearing in the collision operator.
In the simulations we set the following physical parameters $T_e^* = T_i^*$, $\beta_i = 100$, $r_L = 20$, $Z_i = 1$,. Such unphysical mass ratio helps us to save computational resources. The boundary conditions of Poisson's equation are $\phi(z_0) = 0$ and

$$\phi_M(t) = \phi_0 + (\phi_F - \phi_0)\left\{\frac{1}{2} + \frac{1}{\pi}\arctan\left[\omega\left(t - t_0\right)\right]\right\} \qquad \text{(Eq. 10)}$$

Two cases were considered: (i) constant potential with $\phi_0 = \phi_F = -2.75$ and (ii) time-dependent potential with $\phi_0 = -5$, $\phi_F = -2.75$, $t_0 = 500$, and $\omega = 5$. We remark that they present different time histories but provide exactly the same boundary condition in the long term, i.e. a potential value of -2.75 that gives zero net current in the stationary state according to Ref. [2]. The number of points in z- and $v_\parallel$-grids were $N_z = 451$ and $N_v = 77$, respectively and we used $v_{max}^e = 5$ and $v_{max}^i = 0.5$.

3. SIMULATION RESULTS

3.1. Macroscopic Quantities

We here present four simulations. Two of them are collisionless and have Φ_M constant and variable given by (Eq. 10), respectively. The other two have exactly the same conditions, except that there are electron-electron collisions with a collision time equal to $\tau_e = 1000$. This collision time is larger than the typical residence time of reflected and free electrons in the simulation box. The simulations were run up to a time large enough to guarantee that the system reached a stationary state. Such a condition was monitored by plotting the z-profile of certain quantities that are z-independent in stationary conditions, like for instance the ratio j/B, and also the temporal evolution of the density of trapped particles and the temperature at several axial coordinates.

Top panel in Fig. 1 shows the electrostatic potential at the end of the simulation versus the inverse of the magnetic field, which is proportional to the cross-sectional area of the nozzle. The two collisionless simulations with constant and time-dependent ϕ_M, which correspond to solid red and dashed green lines, converge to different steady states. For ϕ_M given by law (Eq. 10) the amount of particles trapped during the transient is larger and it yields a lower value of the electrostatic potential. Interestingly, the two simulations with collisions have exactly the same steady state (dark dashed-dot and blue dotted lines in Fig. 1 overlap). The electron-electron collisions yield a lower value of the electrostatic potential because more particles are trapped (see below) and they also shorten the downstream sheath as compared with the collisionless simulations (see charge density in the bottom panel).

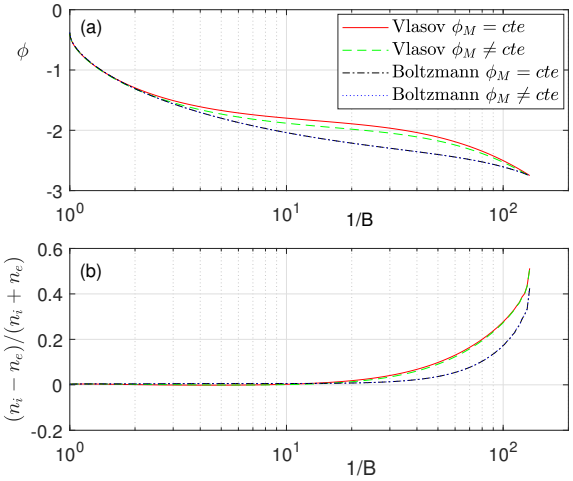

Figure 1: Electrostatic potential (top) and charge density (bottom) versus the inverse of the magnetic field.

The electron parallel and perpendicular temperatures versus $1/B$ for the four simulations are shown in the top and bottom panels of Fig. 2. As expected, the collisions make the distribution function more isotropic because they decrease the parallel temperature and increase the perpendicular one. Interestingly, the temperatures at z_M are almost the same with and without collisions but the z-profiles are totally different. In the collisionless case the parallel temperature is almost constant and drops abruptly in the downstream sheath. For weakly collisional plasmas the parallel electron temperature decreases almost exponentially with the inverse of the magnetic field (note the logarithmic scale in the x-axis).

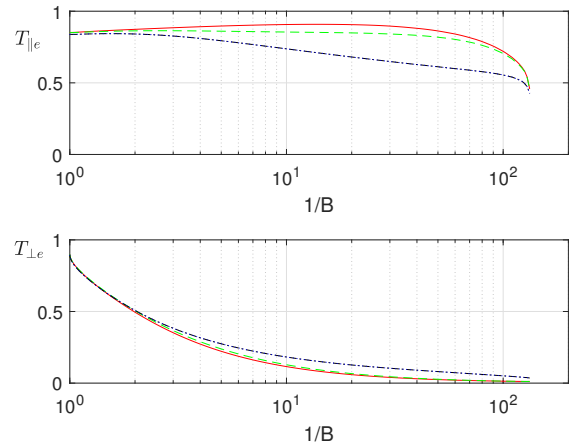

Figure 2: Parallel (top) and perpendicular (bottom) electron temperatures versus the axial coordinate. See legend in Fig. 1.

There are three populations of electrons in the magnetic nozzle: (i) free electrons that have enough energy to leave the simulation box at z_M, (ii) reflected electrons that are injected and leave the simulation box at z_0, and (iii) doubly trapped electrons. The latter population is injected at z_0 and during the transient or due to collisions gets trapped between two axial positions. These three electron population are denoted by subscripts F, R, and T. As shown in Fig. 3, collisions influence considerably the relative composition of the plasma. The ratio of the free electron density to the total density is practically the same for the four simulations (see middle panel). Therefore, it is not affected by the collisions and the time history of ϕ_M. Such a density ratio, and the net current, seems to be controlled by just the final value of Φ_M. The major effect of the collisions is to increase the relative composition of the trapped electron population and decrease the reflected one (see top and bottom panels). The understanding of this feature needs a kinetic analysis made in the next section.

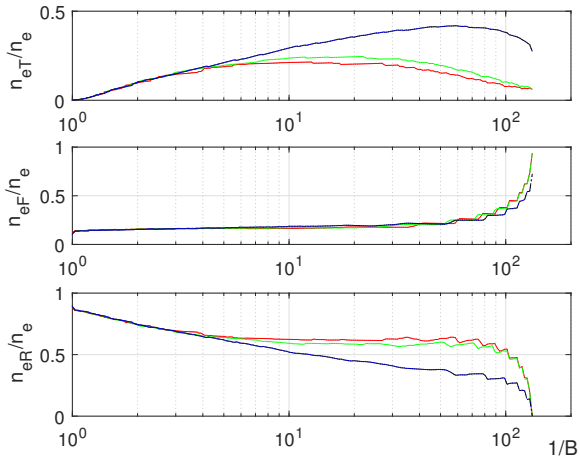

Figure 3: Trapped (top), free (middle), and reflected (bottom) electron densities versus the axial coordinate. See legend in Fig. 1

Figure. 4 shows the evolution of the electron densities (top) and temperatures (bottom) at axial position $z = 90$. As mentioned at the beginning of this section, the system reaches a steady state after the transient phase. The figure also confirms that the simulation time was long enough, and the results presented in this work correspond effectively with steady states.

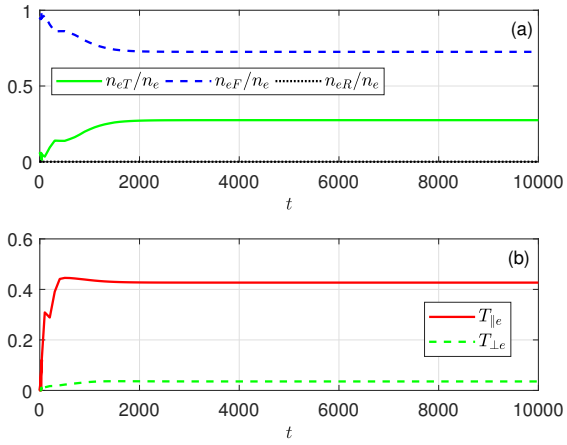

Figure 4: Evolution of the electron densities (top) and temperature (bottom) at $z = 90$. Simulation with collision and constant ϕ_M

3.2. Electron Trapping

The characteristic equations of (Eq. 3) are

$$\frac{dz}{dt} = v_\parallel \qquad \text{(Eq. 11)}$$

$$\frac{dv_\parallel}{dt} = a_\alpha \qquad \text{(Eq. 12)}$$

$$\frac{d\bar{f}_\alpha}{dt} = Q_\alpha^{BGK} \qquad \text{(Eq. 13)}$$

From (Eq. 11) and (Eq. 12) one finds that the energy $E = \beta_\alpha v_\parallel^2/2 + Z_\alpha\phi + \mu B$ is governed by

$$\frac{dE}{dt} = Z_\alpha \frac{\partial \phi}{\partial t} \qquad \text{(Eq. 14)}$$

Therefore, in the steady state with $\partial\phi/\partial t = 0$, the energy is conserved ($dE/dt = 0$). For this reason, certain analyses are easier by changing from $v_\parallel$ to E by using $v_\parallel = \pm\sqrt{2\left(E - Z_\alpha\phi - \mu B\right)/\beta_\alpha}$, and using the parametrization $\bar{f}_\alpha^{\pm}(t, z, E, \mu)$ instead of $\bar{f}_\alpha(t, z, v_\parallel, \mu)$. The $\pm$ signs in the superscript of the distribution function indicate positive and negative axial velocities. The positive and negative distribution functions in the steady state should then satisfy the equation

$$\pm\sqrt{\frac{2\left(E - Z_\alpha\phi - \mu B\right)}{\beta_\alpha}}\frac{\partial \bar{f}_\alpha^{\pm}}{\partial z} = \frac{\bar{f}_{M\alpha}^{\pm} - \bar{f}_\alpha^{\pm}}{\tau_\alpha} \qquad \text{(Eq. 15)}$$

where $\bar{f}_{M\alpha}^{\pm}$ are the Maxwellian distribution function with positive and negative axial velocity in terms of z, μ, and E and we used $dE/dt = d\mu/dt = 0$. According to (Eq. 15) and for a given energy level in the steady state, $\bar{f}_\alpha^{\pm}$ are z-independent piecewise functions in the collisionless case. For weakly collisional plasma ($\tau_\alpha >> 1$), $\bar{f}_\alpha^{\pm}$ are almost constant with z.

The population of trapped particles in the steady state can be identified by plotting the distribution function in a $z - \mu$ plane for a given value of the energy at the end of the simulations. We remark that, at a certain position and energy, the magnetic moment should be smaller than

$$\mu_{max}(z, E) = \frac{E - Z_\alpha\phi(z)}{B(z)} \qquad \text{(Eq. 16)}$$

and a particle is doubly-trapped in the region $z_{min} \leq z \leq z_{max}$ if its magnetic moment μ satisfies $\mu = \mu_{max}(z_{min}, E) = \mu_{max}(z_{max}, E)$. The curve μ_{max} versus z can exhibit a minimum at a certain value of the magnetic moment, say μ^*.

Figure 5 shows the sum of the electron distribution functions $\bar{f}_e^{\pm}$ at the steady state in the $z - \mu$ plane for a given energy level. For convenience, the $\mu_{max} - z$ curve is also presented. Top panels correspond to collisionless simulations and energy levels $E = 2.2$ [panel (a)] and $E = 2.4$ [panel (b)]. It is evident that there are trapped electrons, but they just occupy a relatively narrow μ-band above the minimum of the μ_{max}-curve. Therefore, most of the phase-space region that trapped electrons could potentially occupy is empty. As shown in panels (c) and (d), which present the same results but for a simulation with collisions, the electron-electron collisions change this picture considerably. We first note that the μ_{max}-curves for a given energy level are not the same, because the collisions change the densities and, therefore, the electrostatic potentials in the steady state are different. Moreover, the collisions fill the phase-space region with doubly-trapped electrons, thus explaining the higher density of the trapped electron population presented in Sec. 3.1.. The panels also corroborate a fact already anticipated by (Eq. 15): $\bar{f}^{\pm}$ are z-independent and almost z-independent in the collisionless and weakly collisional cases, respectively.

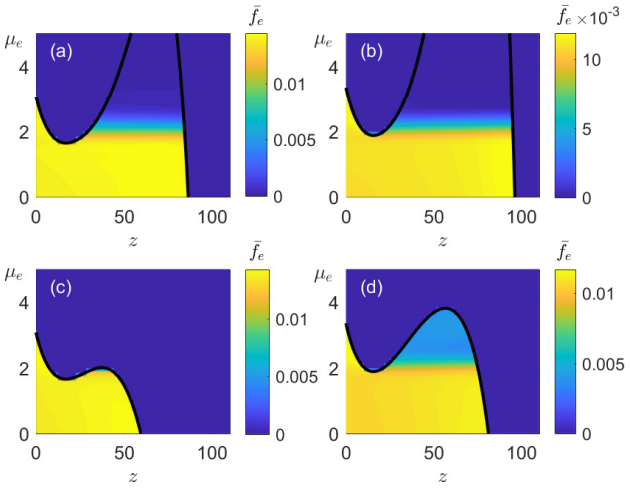

Figure 5: Steady state electron distribution function in the $z - \mu$ plane for a given energy. The top and the low row correspond to collisionless and weakly collisional plasmas, respectively, and left and right columns to $E = 2.2$ and $E = 2.4$.

Figure 6 shows in detail the profiles of the forward and backward distribution function of the electrons for $z = 50$ and $E = 2.4$ in the collionless and weakly collisional simulations [panels (a) and (b) respectively]. These two panels are obtained by making a section at $z = 50$ of Fig. 5.b and 5.d. For convenience, we also plotted the value of μ_{max} for $z = 50$, and the minimum of μ_{max} curve for $E = 2.4$. The distribution functions vanish for $\mu > \mu_{max}$ and the trapped electron region correspond to $\mu^* \leq \mu \leq \mu_{max}$. The panels include the forward and backward Maxwellian distribution functions with density, drift velocity, and temperature equal to the local values of the distribution function obtained in the simulation. These distributions f^+_{Me} and f^-_{Me} are obtained by writting (Eq. 8) as a function of the energy (instead of $v_\parallel$) and they are different because the local value of u_e is not zero. In the collisionless simulation the distribution functions are far from Maxwellian and they decreases abruptly to the right of μ^*, i.e. only a narrow μ-range is filled with trapped electrons [see panel (a)]. Even in the weakly collisional case the distribution functions do not follow a Maxwellian, although they are much closer in the trapped region. Clearly, the collisions increased the amount of trapped electrons.

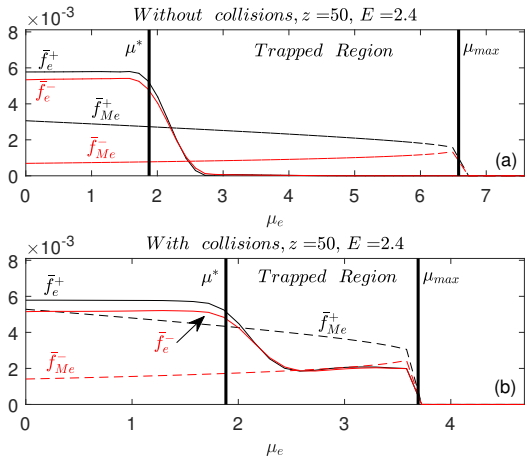

Figure 6: Forward and backward electron distribution functions versus mu for $z = 50$ and $E = 2.4$ in the steady state. The top and the low panel correspond to collisionless and weakly collisional plasmas, respectively.

Figure 7 shows the distribution function of the electrons in the $v_\parallel - \mu$ plane for $z = 50$ [panels (a) and (c)] and $z = 75$ [panels (b) and (d)]. Similarly to Fig. 5, panels (a)-(b) and (c)-(d) correspond to collisionless and weakly collisional simulations, respectively. The presence of collisions yields a long tail of the distribution function for large μ values and nearly zero axial velocity. Since B decreases with z, such a tail is longer as we move from the throat of the nozzle to z_M.

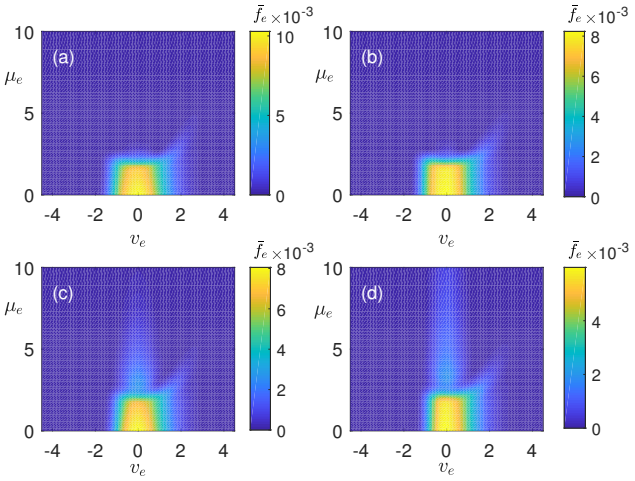

Figure 7: Steady state electron distribution function in the $v_\parallel - \mu$ plane for a given axial coordinate. The top and the bottom row correspond to collisionless and weakly collisional plasmas, respectively, and left and right columns to $z = 50$ and $z = 75$, respectively.

4. CONCLUSIONS

The numerical simulations show that collisions, even if they are rare, play a fundamental role in the steady state of magnetized plasma expansions. The axial profiles of the electrostatic potential and electron temperature are modified considerably. For instance, collisions make the electron parallel temperature decay almost exponentially with the inverse of the magnetic field. Moreover, collisions keep invariant the relative density of free electrons but modify the relative amount of trapped and reflected electrons, respectively. The phase-space region of doubly-trapped electrons is progressively filled by the collisions until a final and unique steady state is reached. Therefore, unlike collisionless plasmas, the simulations suggest that the steady state is unique for weakly collisional plasmas. The equilibrium distribution function is far from Maxwellian, even though the Bhatnagar-Gross-Kook operator is proportional to the difference between the actual distribution function and a Maxwellian with the same local macroscopic properties.

The conclusions of this work are based on a limited number of simulations and may be consolidated by a deeper analysis by varying important physical and numerical parameters such as the collision frequency, the simulation box size, and the downstrean electrostatic potential. We also mention that electron-neutral collisions, ignored in this work, may be dominant for not fully ionized plasma. More refined analysis will be presented in a forthcoming work.

ACKNOWLEDGMENTS

J.Z. was supported by Airbus DS (Grant CW240050). G.S-A was supported by the Ministerio de Economía y Competitividad of Spain (Grant RYC-2014-15357). E.A. was supported by the MINOTOR project, that received funding from the European Union's Horizon 2020 research and innovation programme, under grant agreement 730028. J.R. and M.M-S stays at UC3M for this research were supported by a UC3M-Santander Chair of Excellence and by National R&D Plan (Grant ESP2016-75887), respectively.

A NUMERICAL SCHEME

The simulations have been carried out with an updated version of the code named VLASMAN (VLAsov Simulator for MAgnnetic Nozzle). A detailed description of this code, including mesh in real and velocity space and filtering algorithm to avoid filamentation, can be found in Ref. [2]. We now explain the numerical implementation of the electron collisions, which is the novel feature of this work. For convenience, we write the Boltzmann equation as

$$\frac{\partial f_\alpha}{\partial t} = (\mathcal{S} + \mathcal{F} + \mathcal{C})\, f_\alpha \qquad \text{(Eq. 17)}$$

where the operators for streaming $\mathcal{S}$, forces $\mathcal{F}$, and collisions $\mathcal{C}$ are $\mathcal{S}\bar{f}_\alpha = -v_\parallel \partial \bar{f}_\alpha/\partial z$, $\mathcal{F}\bar{f}_\alpha = -a_\alpha \partial \bar{f}_\alpha/\partial v_\parallel$, and $\mathcal{C}\bar{f}_\alpha = \left(\bar{f}_{M\alpha} - \bar{f}_\alpha\right)/\tau_\alpha$. Our numerical scheme implements a splitting method. Given the distribution functions at time t, the scheme computes it at $t + \Delta t$ by using the following formula [4]

$$\bar{f}_\alpha\left(t_m + \Delta t\right) = C^{1/2} S^{1/2} F S^{1/2} C^{1/2} \bar{f}_\alpha\left(t_m\right) \qquad \text{(Eq. 18)}$$

where for brevity we omitted the dependence with z, $v_\parallel$, and μ of the distribution functions, and $C^{1/2}$, $S^{1/2}$, and F, are operators that propagate the distribution function, according to collisions, streaming and forces, for time steps equal to $\Delta t/2$, $\Delta t/2$, and Δt, respectively.

The collisional part in the splitting method, $\partial \bar{f}_\alpha/\partial t = \mathcal{C}\bar{f}_\alpha$, is discretized with a second-order accuracy in Δt Crank-Nicolson approach [5]

$$C^{1/2}\bar{f}_\alpha(t_m, z, v_\parallel) = \bar{f}_\alpha(t_m, z, v_\parallel) + \frac{1}{2}\frac{\Delta t}{\tau_\alpha + \Delta t/2}\left[\bar{f}_{M\alpha} - \bar{f}_\alpha(t_m, z, v_\parallel\right] \qquad \text{(Eq. 19)}$$

where we omitted again the dependence with μ because it enters as a parameter in the algorithm. The distribution function $\bar{f}_{M\alpha}$ is computed from Eq. 8 and its arguments, n_e, u_e, and T_e, are the macroscopic values of $\bar{f}_\alpha(t_m, z, v_\parallel)$. For the inner part of Eq. 18, i.e. streaming and force ($S^{1/2} F S^{1/2}$), we used the well-known second order scheme [6]

$$S^{1/2}\bar{f}_\alpha(t_m, z, v_\parallel) = \bar{f}_\alpha(t_m, z - v_\parallel \Delta t/2, v_\parallel) \qquad \text{(Eq. 20)}$$

$$F\bar{f}_\alpha(t_m, z, v_\parallel) = \bar{f}_\alpha\left(z, v_\parallel - a_\alpha \Delta t\right) \qquad \text{(Eq. 21)}$$

At each time step, the electric field appearing in a_α is found by solving Poisson's equation with the densities computed from the distribution function $S^{1/2} C^{1/2} \bar{f}$.

REFERENCES

[1] Martinez-Sanchez, M., Navarro-Cavallé, J., and Ahedo, E., "Electron cooling and finite potential drop in a magnetized plasma expansion," *Physics of Plasmas*, Vol. 22, No. 5, 2015, pp. 053501.

[2] Sánchez-Arriaga, G., Zhou, J., Ahedo, E., Martínez-Sánchez, M., and Ramos, J., "Kinetic features and non-stationary electron trapping in paraxial magnetic nozzles," *Plasma Sources Science and Technology*, Vol. 27, No. 3, 2018, pp. 035002.

[3] Bhatnagar, P. L., Gross, E. P., and Krook, M., "A Model for Collision Processes in Gases. I. Small Amplitude Processes in Charged and Neutral One-Component Systems," *Phys. Rev.*, Vol. 94, May 1954, pp. 511–525.

[4] Schiller, U. D., "A unified operator splitting approach for multi-scale fluid–particle coupling in the lattice Boltzmann method," *Computer Physics Communications*, Vol. 185, No. 10, 2014, pp. 2586 – 2597.

[5] Dellar, P. J., "An interpretation and derivation of the lattice Boltzmann method using Strang splitting," *Computers & Mathematics with Applications*, Vol. 65, No. 2, 2013, pp. 129 – 141, Special Issue on Mesoscopic Methods in Engineering and Science (ICMMES-2010, Edmonton, Canada).

[6] Cheng, C. and Knorr, G., "The integration of the vlasov equation in configuration space," *Journal of Computational Physics*, Vol. 22, No. 3, 1976, pp. 330 – 351.